Applied Physics Letters

hBN-based enhancement and regulation of radiative heat transfer between two monolayer graphene sheets

Cite as: Appl. Phys. Lett. **121**, 171104 (2022); https://doi.org/10.1063/5.0117028
Submitted: 30 July 2022 • Accepted: 07 October 2022 • Published Online: 27 October 2022

Jinlin Song, Lei Chen, Lin Jin, et al.

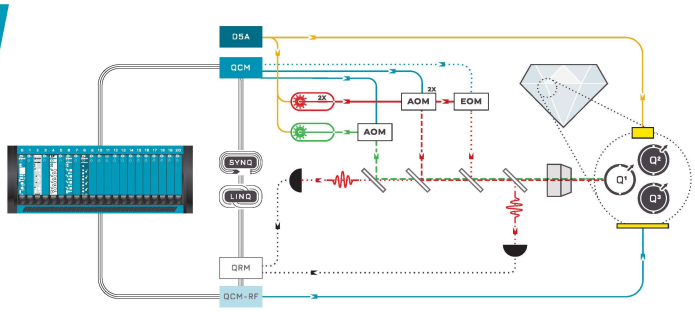

Applied Physics Letters ARTICLE scitation.org/journal/apl

hBN-based enhancement and regulation of radiative heat transfer between two monolayer graphene sheets

Cite as: Appl. Phys. Lett. **121**, 171104 (2022); doi: 10.1063/5.0117028
Submitted: 30 July 2022 · Accepted: 7 October 2022 ·
Published Online: 27 October 2022

Jinlin Song,[1,a)] Lei Chen,[1] Lin Jin,[1] Lei Yao,[1] Humeyra Caglayan,[2] and Run Hu[3,a)]

AFFILIATIONS

[1]School of Electrical and Information Engineering, Wuhan Institute of Technology, Wuhan 430205, Hubei, People's Republic of China
[2]Faculty of Engineering and Natural Sciences, Tampere University, 33720 Tampere, Finland
[3]State Key Laboratory of Coal Combustion, School of Energy and Power Engineering, Huazhong University of Science and Technology, Wuhan 430074, Hubei, People's Republic of China

Note: This paper is part of the APL Special Collection on Thermal Radiation at the Nanoscale and Applications.
[a)]**Authors to whom correspondence should be addressed:** songjinlin@wit.edu.cn and hurun@hust.edu.cn

ABSTRACT

Near-field radiative heat transfer (NFRHT) in many-body systems has opened pathways for enabling novel thermal-radiation applications. In this Letter, we investigate hBN-based enhancement and regulation of NFRHT between two monolayer graphene sheets. On the one hand, we predict that adding an intermediate hBN plate can greatly compensate the exponential damping of evanescent waves due to its hyperbolic modes, thus leading to 1.5 times enhancement of the NFRHT without introducing additional thermal source compared to the graphene-graphene system. On the other hand, we find that adjusting the shift frequency of hBN can greatly change the coupling of its hyperbolic modes and graphene surface plasmon polaritons, thus enabling the remarkable thermal regulation with a ratio of 3.5. We hope that our work may facilitate nanoscale thermal management in many-body systems and benefit the comprehension of hBN-based photon tunneling.

Due to the huge contribution of evanescent wave coupling, near-field radiative heat transfer (NFRHT) can exceed the blackbody limit by several orders of magnitude when the separation distance between two objects is less than the characteristic wavelength of thermal radiation (about 10 μm at room temperature).[1–4] Therefore, on the one hand, thanks to the ultrahigh heat flux, NFRHT has great potentials in thermophotovoltaics, thermal microscopy, heat-assisted magnetic recording, and radiative cooling;[5–10] on the other hand, accompanied by the rapid development of advanced nanotechnology, NFRHT has become a ubiquitous phenomenon in integrated nanoscale electronics and optoelectronics nowadays, which may remarkably influence the device performance and durability.[11] Consequently, the enhancement and regulation of NFRHT, especially in terms of many-body systems having at least three objects participating in heat transfer, has attracted special attention recently.[12–17] Compared to two-body systems, many-body systems are more usual in nature, and the inborn mutual interactions among multiple objects are significant to be well understood and utilized for practical applications.[18,19] The recent decade has witnessed a plethora of theoretical and experimental achievements on many-body NFRHT to realize the enhancement and regulation of radiative heat transfer in the planar geometry. Messina *et al.* have theoretically predicted that, adding an intermediate plate between two plates can partially alleviate the intrinsic exponential damping in vacuum due to three-body mutual interactions, thus allowing for the remarkable amplification of radiative heat transfer.[20] This kind of enhancement can be further improved by using hyperbolic metamaterials and constructing periodic gratings.[21,22] Combing with adjustable materials, like graphene, phase change materials like VO_2 and so on, many applications, including thermal transistor, thermal memory, modulator, and thermostat, can be realized.[23–27]

Hexagonal boron nitride (hBN) is a kind of natural hyperbolic materials, which supports hyperbolic modes (HMs) with high-k modes in its two Reststrahlen bands in the mid-infrared. It is a competitive candidate material for high-performance near-field optical imaging and focusing[28,29] and also has a high carrier mobility to be used as the substrate of graphene and other materials.[30]

These reasons inspired researchers to extensively and intensively investigate the NFRHT of hBN in recent years.[31–34] Researchers have predicted that, the HMs in hBN can couple with the adjustable graphene surface plasmon polaritons (GSPPs), making it possible to regulate the NFRHT between graphene-coated hBN systems and between multilayer graphene-hBN heterostructures.[33,34] Very recently, Latella *et al.*[35] proposed to tailor the strain-induced shift frequency of hBN to control NFRHT. However, the mutual interactions of photon tunneling in hBN-based many-body systems still need to be further explored to enhance and regulate the radiative heat transfer.

In view of this, we theoretically investigate the NFRHT between two monolayer graphene sheets mediated by an hBN plate. We show that, the intermediate hBN plate not only greatly enhances the radiative heat flux but also endows the heat transfer between two monolayer graphene sheets with high tunablity by adjusting the shift frequency. Our work may find applications in nanoscale thermal management and facilitate the understanding of hBN-based photon tunneling in many-body systems.

As shown in Fig. 1(a), the considered three-body system includes two monolayer graphene sheets (indexed by 1 and 3) and the intermediate hBN plate (indexed by 2). In this Letter, the thicknesses of the graphene sheet and hBN plate are $t_g = 0.5$ and $t = 110$ nm, respectively, while the adjacent plates are separated by vacuum gaps of $d = 20$ nm. The temperatures of two terminal graphene sheets are, respectively, fixed at $T_1 = 400$ and $T_3 = 300$ K. The optical axis of hBN is assumed in the z direction, so that its permittivity tensor with uniaxial anisotropy reads $\hat{\varepsilon} = \mathrm{diag}(\varepsilon_O, \varepsilon_O, \varepsilon_E)$, where the subscripts O and E stand for the ordinary (the electric field is perpendicular to the optical axis) and extraordinary (the electric field is parallel to the optical axis) components, respectively.[36] The strain-induced shift frequency into phonon frequency can separately or simultaneously modify ε_O and ε_E.[37,38] More specifically, a compressive strain will shift the hBN phonon to a higher frequency, and a tensile strain will shift the hBN phonon to a lower frequency. Here, we only consider tuning the shift frequency by the tensile strain and focus on the regulation of NFRHT due to the simultaneous modification of ε_O and ε_E on NFRHT in such a three-body system. In this scenario, the permittivity of hBN can be expressed as[35]

$$\varepsilon_{l,\Omega} = \varepsilon_{\infty,l}\frac{(\omega_{\mathrm{LO},l}-\Omega)^2-\omega^2-i\gamma_l\omega}{(\omega_{\mathrm{TO},l}-\Omega)^2-\omega^2-i\gamma_l\omega}, \tag{1}$$

where $\varepsilon_{l,\Omega}$ is the high-frequency permittivity having l = O or E, Ω is the shift frequency, and γ_l is the damping constant. $\omega_{\mathrm{TO},l}$ and $\omega_{\mathrm{LO},l}$, respectively, stand for the transverse phonon frequency and longitudinal phonon frequency, while $\omega_{\mathrm{TO,O}} = 1370$ and $\omega_{\mathrm{LO,O}} = 1610$, and $\omega_{\mathrm{TO,E}} = 780$ and $\omega_{\mathrm{LO,E}} = 830$ cm^{-1}. In addition, the other parameters are $\varepsilon_{\infty,\mathrm{O}} = 4.87$, $\gamma_\mathrm{O} = 5$, $\varepsilon_{\infty,\mathrm{E}} = 2.95$, and $\gamma_\mathrm{E} = 4$ cm^{-1}.[29,39] Obviously, when $\Omega = 0$, Eq. (1) reduces to the intrinsic form of hBN, which reads $\varepsilon_l = \varepsilon_{\infty,l}\frac{\omega_{\mathrm{LO},l}^2-\omega^2-i\gamma_l\omega}{\omega_{\mathrm{TO},l}^2-\omega^2-i\gamma_l\omega}$. Figure 1(b) shows the permittivity of intrinsic hBN for three shift frequencies: $\Omega = 0$, $\Omega = 0.7\times10^{14}$, and $\Omega = 1.4\times10^{14}$ rad s^{-1}. It can be seen that, the intrinsic hBN supports HMs with $\varepsilon_O > 0$ and $\varepsilon_E < 0$ (type I) from 1.47×10^{14} to 1.56×10^{14} rad s^{-1}, and HMs with $\varepsilon_O < 0$ and $\varepsilon_E > 0$ (type II) from 2.58×10^{14} to 3.03×10^{14} rad s^{-1}. With the increase in Ω, types I and II HMs both move to lower frequencies, making hBN possible to regulate the NFRHT.

With regard to such a three-body planar system, according to the fluctuation-dissipation theorem, the near-field radiative heat flux between the terminal plates can be expressed as[20]

$$Q(\omega,T) = \frac{1}{4\pi^2}\sum_j\int_0^\infty\int_0^\infty\{[\Theta(\omega,T_1)-\Theta(\omega,T_2)]\xi_{12}^j + [\Theta(\omega,T_2)-\Theta(\omega,T_3)]\xi_{23}^j\}\,\beta d\,\beta d\,\omega, \tag{2}$$

where j = TM or TE represents the polarization, $\Theta(\omega,T_n) = \hbar\omega/[\exp(\hbar\omega/k_BT_n)-1]$ is the Planck harmonic oscillator of body n, and β is the parallel wavevector component. ξ_{12}^j (ξ_{23}^j) is the energy transmission coefficient between bodies 1 and 2 (bodies 2 and 3), which evaluate the probability of photon tunneling through the vacuum gap in the three-body system. They can be expressed as

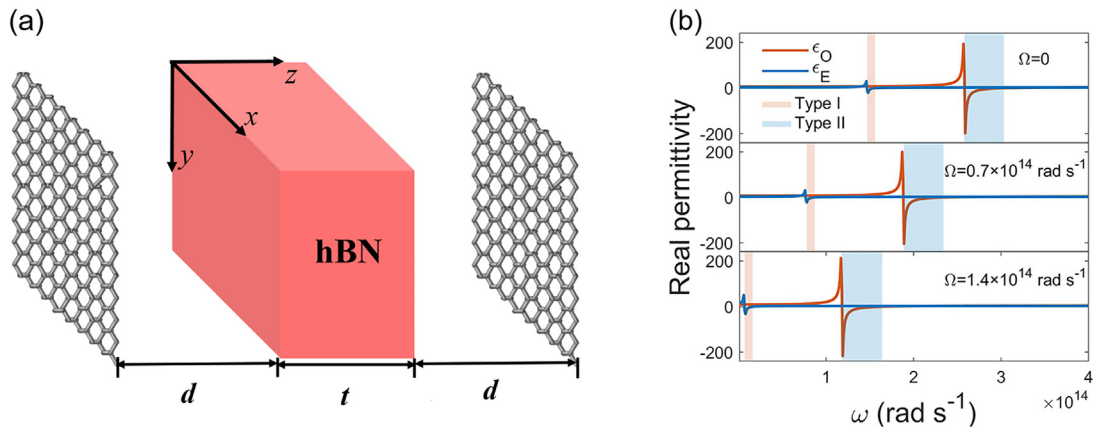

FIG. 1. (a) Schematic illustration of the graphene-hBN-graphene (termed as G-hBN-G) system in this work. The separation distances between adjacent plates are equal to d, and the thickness of the hBN plate is t. (b) Real parts of permittivity of hBN for three shift frequencies: $\Omega = 0$, $\Omega = 0.7\times10^{14}$, and $\Omega = 1.4\times10^{14}$ rad s^{-1}. The red and blue areas mark types I and II hyperbolic frequency regions, respectively.

$$\xi_{12}^{j}=\begin{cases}\dfrac{|\tau_2^j|^2(1-|\rho_1^j|^2)(1-|\rho_3^j|^2)}{|1-\rho_{12}^j\rho_3^j e^{-2\mathrm{Im}(k_{z0})d}|^2|1-\rho_1^j\rho_2^j e^{-2\mathrm{Im}(k_{z0})d}|^2}, & \beta<\dfrac{\omega}{c}\\ \dfrac{4|\tau_2^j|^2\mathrm{Im}(\rho_1^j)\mathrm{Im}(\rho_3^j)e^{-4\mathrm{Im}(k_{z0})d}}{|1-\rho_{12}^j\rho_3^j e^{-2\mathrm{Im}(k_{z0})d}|^2|1-\rho_1^j\rho_2^j e^{-2\mathrm{Im}(k_{z0})d}|^2}, & \beta>\dfrac{\omega}{c}\end{cases}, \quad (3)$$

$$\xi_{23}^{j}=\begin{cases}\dfrac{(1-|\rho_{12}^j|^2)(1-|\rho_3^j|^2)}{|1-\rho_{12}^{p,s}\rho_3^{p,s}e^{-2\mathrm{Im}(k_{z0})d}|^2}, & \beta<\dfrac{\omega}{c}\\ \dfrac{4\mathrm{Im}(\rho_{12}^j)\mathrm{Im}(\rho_3^j)e^{-2\mathrm{Im}(k_{z0})d}}{|1-\rho_{12}^j\rho_3^j e^{-2\mathrm{Im}(k_{z0})d}|^2}, & \beta>\dfrac{\omega}{c}\end{cases}, \quad (4)$$

where ρ_n^j and τ_n^j are, respectively, the reflection and transmission coefficients of body n, $k_{z0}=\sqrt{\omega^2/c^2-\beta^2}$ is the vacuum wave vector in the z direction, c_0 is the light velocity in vacuum, and Im denotes the imaginary part. $\rho_{12}^j=\rho_2^j+\frac{\rho_1^j(\tau_2^j)^2e^{-2\mathrm{Im}(k_{z0})d}}{1-\rho_1^j\rho_2^j e^{-2\mathrm{Im}(k_{z0})d}}$ is the reflection coefficient of an entity consisting of bodies 1 and 2. According to thin film optics,[40] the reflection coefficient and transmission coefficient of each plate are $\rho_n^j=\frac{r_{0n}^j-r_{0n}^j e^{-2\mathrm{Im}(k_{zn}^j)t_n}}{1-(r_{0n}^j)^2e^{-2\mathrm{Im}(k_{zn}^j)t_n}}$ and $\tau_n^j=\frac{(1-(r_{0n}^j)^2)e^{-\mathrm{Im}(k_{zn}^j)t_n}}{1-(r_{0n}^j)^2e^{-2\mathrm{Im}(k_{zn}^j)t_n}}$, respectively. $r_{0n}^{\mathrm{TM}}=\frac{\varepsilon_{On}k_{z0}^{\mathrm{TM}}-k_{zn}^{\mathrm{TM}}}{\varepsilon_{On}k_{z0}^{\mathrm{TM}}+k_{zn}^{\mathrm{TM}}}$ and $r_{0n}^{\mathrm{TE}}=\frac{k_{z0}^{\mathrm{TE}}-k_{zn}^{\mathrm{TE}}}{k_{z0}^{\mathrm{TE}}+k_{zn}^{\mathrm{TE}}}$ are the Fresnel reflection coefficients of body n for TM and TE waves, respectively, where $k_{zn}^{\mathrm{TM}}=\sqrt{k_0^2\varepsilon_{On}-\beta^2\varepsilon_{On}/\varepsilon_{En}}$ and $k_{zn}^{\mathrm{TE}}=\sqrt{k_0^2\varepsilon_{On}-\beta^2}$ are z-component wavevectors.

Because the variation in the intermediate plate thickness in a three-body system has twofold effects, it changes the gap spacing while changing the thickness, and the effect of strain-induced deformation quantity of the intermediate plate on the heat transfer in such a three-body system becomes more obvious, e.g., the total heat flux in the G-hBN-G system has a difference of ~10% when the thickness difference equals 5%, which are not shown here. However, for ease of direct comparison with the G-hBN and G–G systems, we still neglect the strain-induce deformation quantity in this work. Subsequently, we investigate the effects of the shift frequency on the total radiative heat flux, as shown in Fig. 2(a). In the G–G system with the separation distance of 150 nm for $\mu=0.1$ eV, Q equals 9.8×10^4 W m^{-2}. In the G-hBN-G system for $\mu=0.1$ eV, the terminal graphene sheets are also separated by 150 nm. In this case, Q reaches 1.5×10^5 W m^{-2}, which is almost 1.5 times larger than that of the G–G system in the intrinsic state when $\Omega=0$, demonstrating the enhancement of the NFRHT in such a three-body system. With the increase in Ω, Q rises monotonically and shows the maximum value of 5.4×10^5 W m^{-2} when $\Omega=1.5\times10^{14}$ rad s^{-1}. However, Q slightly increases first and then gradually decreases for $\mu=0.2$ eV, and even almost has no change for $\mu\geq0.3$ eV. It is noteworthy that, in the G-hBN-G system, the hBN plate temperature is set to be 360.3 K to make the flux on it vanish to avoid the introduction of a supplementary thermal source. In contrast to the above two kinds of systems, the G-hBN system is asymmetric and has distinct optical properties on two sides, so Qs for $\mu=0.1$ and 0.2 eV show much less values of 1.2×10^4 and 1.6×10^4 W m^{-2} when $\Omega=0$ and seem independent of Ω. In this Letter, we define the regulation ratio as $\alpha=Q_{\max}/Q_{\min}$, where $Q_{\max}$ and $Q_{\min}$ are in the same chemical potential, in order to quantitatively evaluate the thermal regulation. For the G-hBN-G system with $\mu=0.1$ eV, α can reach above 3.5, suggesting a remarkable thermal regulation effect by adjusting the shift frequency of hBN. For the G-hBN system with $\mu=0.1$ eV, α equals 1.2, indicating that the G-hBN-G system is superior to the G-hBN system in terms of thermal regulation.

The spectral heat fluxes in the G-hBN-G, G-hBN, and G–G systems for $\mu=0.1$ eV are shown in Fig. 2(b). It can be seen that, q_ω in the G–G system has only a broad peak around $\omega=1\times10^{14}$ rad s^{-1}. However, when the intermediate hBN plate of $\Omega=0$ (i.e., hBN is intrinsic) is added, this heat flux peak becomes narrow, and the other two peak occurs at 1.56×10^{14} rad s^{-1} and near 3×10^{14} rad s^{-1}, which matches with types I and II hyperbolic regions of hBN. When Ω increases to 1.4×10^{14} rad s^{-1} due to the redshift of types I and II HMs, q_ω in the G-hBN-G system has two pronounced broad peaks, one near 0.5×10^{14} rad s^{-1} and the other near 1.5×10^{14} rad s^{-1},

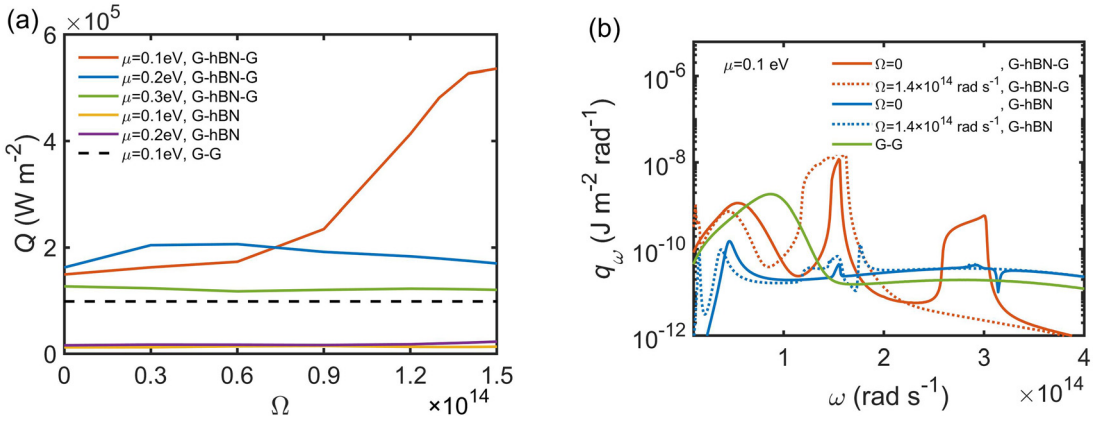

FIG. 2. (a) Total radiation heat fluxes Q in the G-hBN-G systems as a function of the shift frequency of hBN with $\mu=0.1$, 0.2, and 0.3 eV. The total radiation heat fluxes in the graphene-hBN (termed as G-hBN) system with $\mu=0.1$ and 0.2 eV and the graphene-graphene (termed as G–G) system with $\mu=0.1$ eV are shown for comparison. (b) Spectral heat fluxes q_ω in the G-hBN-G and G-hBN systems when $\Omega=0$ and $\Omega=1.4\times10^{14}$ rad s^{-1} for $\mu=0.1$ eV and in the G–G system for $\mu=0.1$ eV. The vacuum gap distance is $d=20$ nm, and the hBN plate thickness is $t=110$ nm.

which are closer to the peak frequency of the Planck flux spectrum. As a result, Q reaches 5.3×10^5 W m^{-2}, which is higher than that when $\Omega = 0$. In the G-hBN system, q_ω shows a much less value, whose small peaks have small change, so the shift frequency nearly has little effect on the NFRHT.

To further elucidate the underlying mechanisms of the hBN-based enhancement of NFRHT in the G-hBN-G system, Figs. 3(a) and 3(b), respectively, give the TM-polarized energy transmission coefficients in the G–G and G-hBN-G systems for $\mu = 0.1$ eV. (TE waves are ignored due to their negligible contribution.) For the G-hBN-G system, we give $\xi_{3B}^{TM} = (\xi_{12}^{TM} + \xi_{23}^{TM})/2$ to analyze its photon tunneling. It can be seen in Fig. 3(a) that, there exist two apparent bands with high photon tunneling probability, which split at low β while merge at large β and can be derived by the coupled GSPPs as follows:[41]

$$1 + \frac{\sigma k_{z0}}{\omega \varepsilon_0} = \coth\left(\frac{ik_{z0}d}{2}\right), \quad \text{symmetric branch,} \tag{5}$$

$$1 + \frac{\sigma k_{z0}}{\omega \varepsilon_0} = \tanh\left(\frac{ik_{z0}d}{2}\right), \quad \text{antisymmetric branch.} \tag{6}$$

The symmetric branch at low frequencies and the antisymmetric branch at high frequencies agree well with q_ω in the G–G system in Fig. 2(b). In the presence of the intermediate intrinsic hBN plate, types I and II HMs occur at high frequencies. Type I HMs support a large β up to $150k_0$, leading to a high heat flux peak at 1.56×10^{14} rad s^{-1}. Type II HMs are featured by the multiple branches merge at high β values due to the existence of the hBN interfaces. The GSPPs, slightly compressed by type I HMs, accompanied by types I and II HMs, dominate the NFRHT in different frequency regions, resulting in three isolated heat flux peaks as shown in Fig. 2(b). According to Eq. (3), the transmission coefficient τ_2^j of the hBN plate in the numerator plays a key role in ξ_{12}^j. If the intermediate medium is vacuum, then $\tau_2^j = 1$ and $\rho_2^j = 0$ so that $\rho_{12}^j = \rho_1^j e^{-2\mathrm{Im}(k_{z0})d}$. In this scenario, the three-body problem reduces to the two-body problem with the separation distance of $2d + t$. Here, we give $|\tau_2|$ for TM waves in Fig. 2(c). We find that, $|\tau_2^{TM}| > 1$ in the two hyperbolic regions of hBN. Note that, the maximum $|\tau_2^{TM}|$ even reaches 25 in the type II hyperbolic region. This suggests that the hBN plate compensates the exponential damping of evanescent waves in vacuum due to its HMs, thus leading to enhancement of the NFRHT.

In the G-hBN system with $\mu = 0.1$ eV, there exist two indistinct bands denoting the adjustable HMs for different Ω, as shown in Figs. 4(a) and 4(b). In this case, the GSPPs are unable to couple with the HMs in hBN and, thus, have negligible contribution to the heat transfer. In the G-hBN-G system when $\Omega = 1.4 \times 10^{14}$ rad s^{-1}, the GSPPs couple with type I HMs of hBN at low frequencies, while type II HMs move to around 1.5×10^{14} rad s^{-1} as shown in Fig. 4(c).

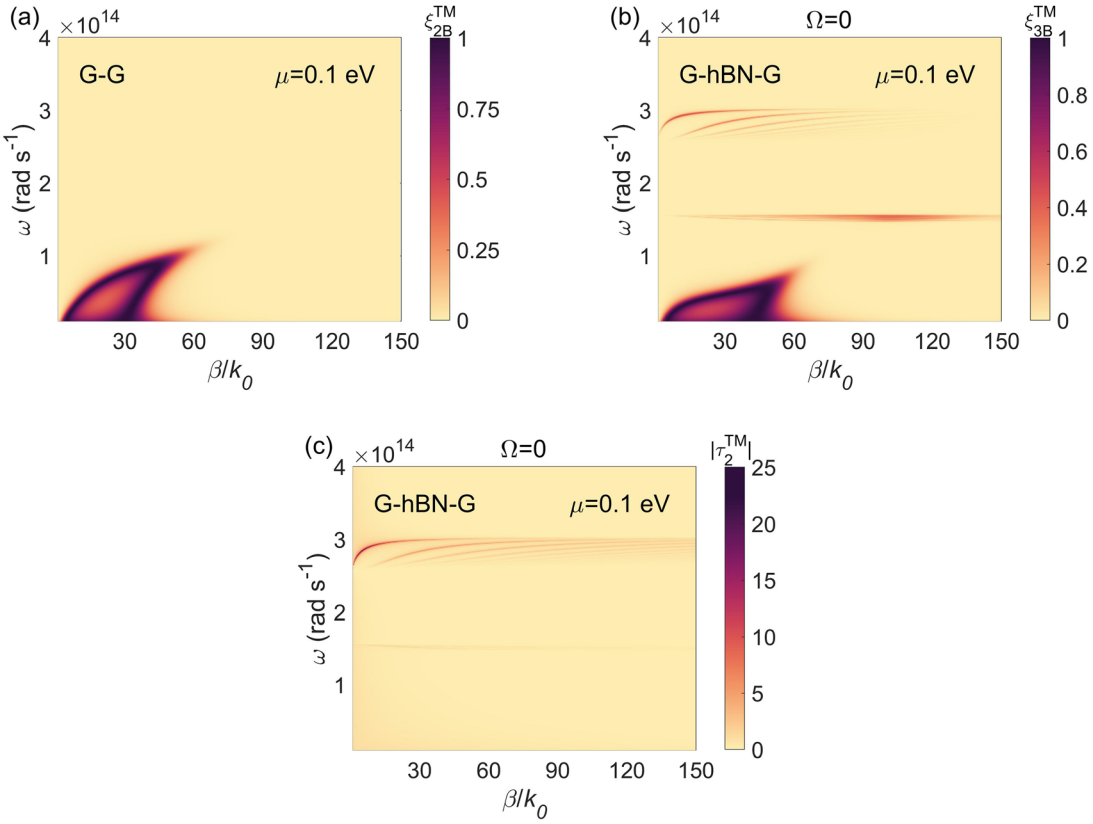

FIG. 3. (a) Energy transmission coefficients ξ_{2B}^{TM} in the G–G system. (b) and (c) Energy transmission coefficient ξ_{3B}^{TM} in the G-hBN-G system when $\Omega = 0$ and the corresponding transmission coefficient $|\tau_2^{TM}|$ of the hBN plate. In the G-hBN-G (G–G) system, the vacuum gap distance is $d = 20$ nm (150 nm), and the hBN plate thickness is $t = 110$ nm. The chemical potential of graphene is fixed as $\mu = 0.1$ eV.

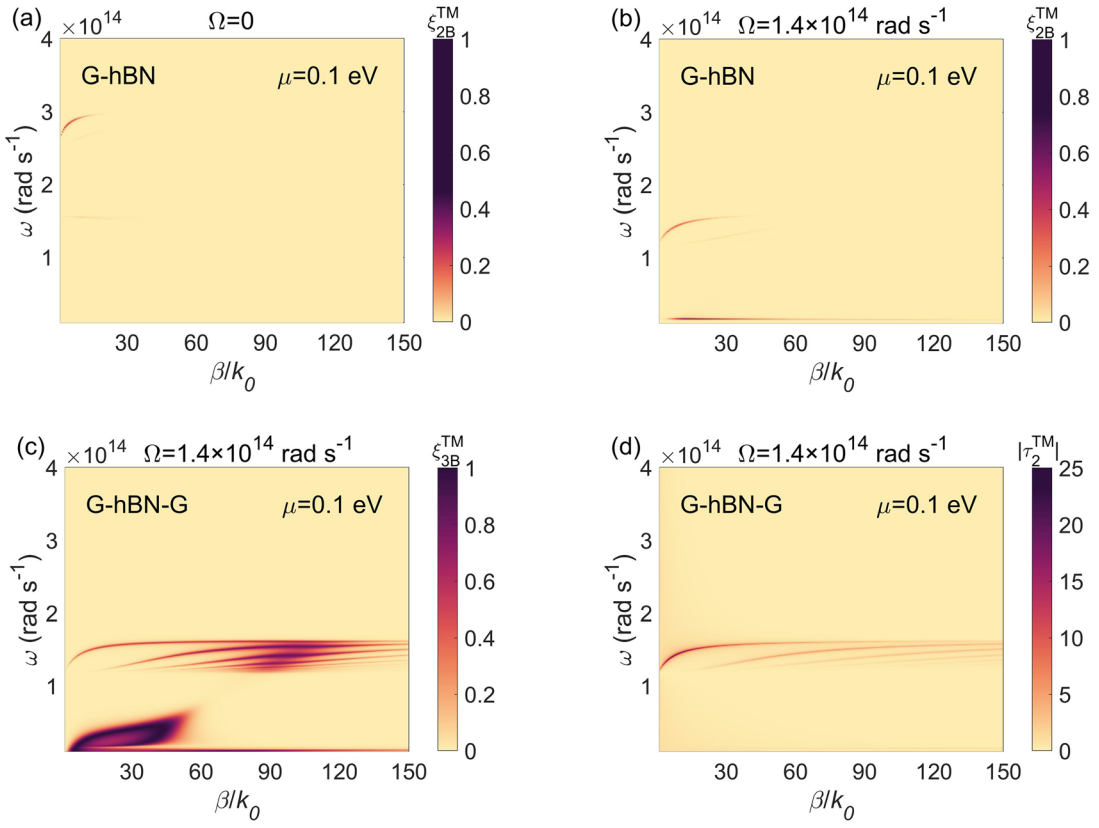

FIG. 4. (a) and (b) Energy transmission coefficients ξ_{2B}^{TM} in the G-hBN system when $\Omega = 0$ and $\Omega = 1.4 \times 10^{14}$ rad s^{-1}. (c) and (d) Energy transmission coefficient ξ_{3B}^{TM} in the G-hBN-G system when $\Omega = 1.4 \times 10^{14}$ rad s^{-1} and the corresponding transmission coefficient $|\tau_2^{TM}|$ of the hBN plate. In the G-hBN-G (G-hBN) system, the vacuum gap distance is $d = 20$ nm (150 nm), and the hBN plate thickness is $t = 110$ nm. The chemical potential of graphene is fixed as $\mu = 0.1$ eV.

This explains the two broad heat flux peaks in Fig. 2(b). Compared to the case when $\Omega = 0$ as shown in Fig. 3(b), ξ_{3B}^{TM} when $\Omega = 1.4 \times 10^{14}$ rad s^{-1} have higher values at frequencies closer to the peak frequency of the Planck flux spectrum, thus endowing the heat flux of the G-hBN-G system with high tunability. In addition, the transmission coefficient $|\tau_2^{TM}|$ of the hBN plate is shown in Fig. 4(d). The enhanced transmission due to type II HMs can be clearly seen which shows the maximum value close to 25, while type I HMs almost vanish.

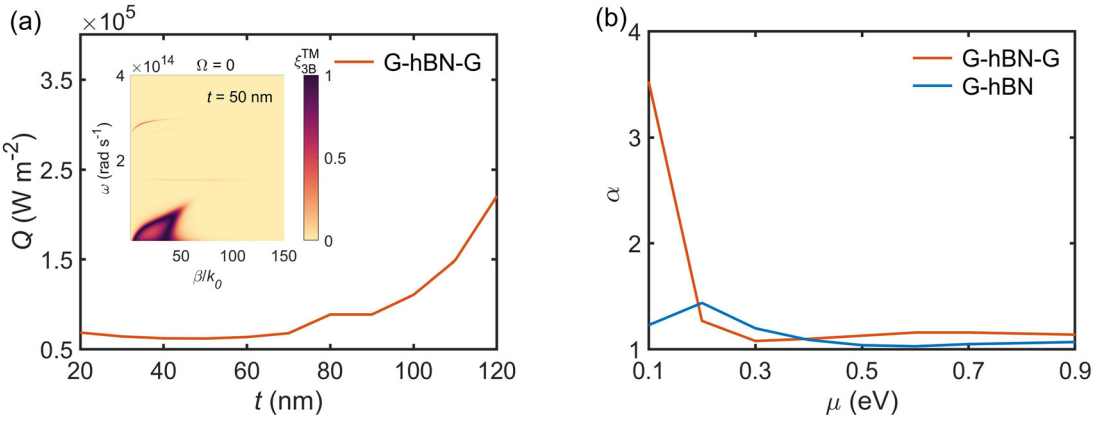

FIG. 5. (a) Total radiative heat fluxes Q in the G-hBN-G system as a function the intermediate hBN plate thickness for $\mu = 0.1$ eV when $2d + t$ is fixed as 150 nm. The inset gives the energy transmission coefficients ξ_{3B}^{TM} in the G-hBN-G system when $\Omega = 0$ and $t = 50$ nm. (b) Regulation ratios α vs the graphene chemical potential μ in the G-hBN-G and G-hBN systems. In the G-hBN-G (G-hBN) system, the vacuum gap distance is $d = 20$ nm (150 nm), and the hBN plate thickness is $t = 110$ nm.

Figure 5(a) illustrates the total radiation heat fluxes Q in the G-hBN-G system as a function the intermediate hBN plate thickness for $\mu = 0.1$ eV with $2d + t$ being 150 nm. In general, Q increases from 0.7×10^5 W m^{-2} when $t = 20$ nm to 2.2×10^5 W m^{-2} when $t = 120$ nm. Comparing the inset which shows ξ_{3B}^{TM} when $t = 50$ nm with Fig. 3(b), it can be seen that, a thicker hBN plate can provide more intense photon tunneling due to HMs, so leading to a higher heat flux. Figure 5(b) gives the regulation ratios α as a function of the μ in the G-hBN-G and G-hBN systems. In the G-hBN-G system, α shows the maximum value of 3.5 for $\mu = 0.1$ eV. It sharply declines to 1.3 for $\mu = 0.2$ eV and then undergoes little change with the increase in μ. In the G-hBN system, α reaches the maximum value of 1.4 for $\mu = 0.2$ eV and then tends to be stable. In addition, the G-hBN-G system is almost superior to the G-hBN system in terms of thermal regulation except for $\mu = 0.2$ and 0.3 eV, and a better regulation performance may be obtained in such kinds of graphene-mediated systems with low μ.

In summary, we theoretically investigate the NFRHT in a three-body system consisting of two monolayer graphene sheets and an intermediate hBN plate. On the one hand, we predict that, adding an hBN plate can greatly compensate the exponential damping of evanescent waves due to its HMs, thus leading to 1.5 times enhancement of the NFRHT without introducing additional thermal source compared to the G–G system. On the other hand, we find that adjusting the shift frequency of hBN can greatly change the coupling of its HMs and GSPPs, thus enabling the remarkable thermal regulation with the ratio of 3.5. Note that, if the hBN plate thickness is extremely large, e.g., close to 150 nm, the radiative heat transfer becomes complicated and may undergo the crossover regime between conduction and radiation.[42] We hope that our work may facilitate nanoscale thermal management in many-body systems and benefit the comprehension of hBN-based photon tunneling in the near future.

The authors acknowledge financial support from the Startup Program of Wuhan Institute of Technology (No. K2021026), the Open Foundation of State Key Laboratory of Coal Combustion, and the National Natural Science Foundation of China (NSFC) (No. 52211540005).

AUTHOR DECLARATIONS

Conflict of Interest

The authors have no conflicts to disclose.

Author Contributions

Jinlin Song: Conceptualization (lead); Funding acquisition (lead); Methodology (lead); Supervision (lead); Writing – review & editing (lead). **Lei Chen:** Data curation (lead); Investigation (lead); Writing – original draft (equal). **Lin Jin:** Project administration (equal); Validation (equal). **Lei Yao:** Project administration (equal); Validation (equal). **Humeyra Caglayan:** Investigation (equal). **Run Hu:** Funding acquisition (equal); Project administration (equal); Supervision (equal).

DATA AVAILABILITY

The data that support the findings of this study are available from the corresponding authors upon reasonable request.

REFERENCES

[1]Z. M. Zhang, *Nano/Microscale Heat Transfer* (McGraw-Hill, New York, 2007).
[2]L. M. Woods, D. A. R. Dalvit, A. Tkatchenko *et al.*, "Materials perspective on Casimir and van der Waals interactions," Rev. Mod. Phys. **88**(4), 045003 (2016).
[3]A. I. Volokitin and B. N. J. Persson, "Near-field radiative heat transfer and noncontact friction," Rev. Mod. Phys. **79**(4), 1291 (2007).
[4]M. Lim, J. Song, S. S. Lee, *et al.*, "Tailoring near-field thermal radiation between metallo-dielectric multilayers using coupled surface plasmon polaritons," Nat. Commun. **9**(1), 4302 (2018).
[5]G. R. Bhatt, B. Zhao, S. Roberts *et al.*, "Integrated near-field thermo-photovoltaics for heat recycling," Nat. Commun. **11**(1), 2545 (2020).
[6]A. Fiorino, L. Zhu, D. Thompson *et al.*, "Nanogap near-field thermophotovoltaics," Nat. Nanotechnol. **13**(9), 806–811 (2018).
[7]B. Zhao, P. Santhanam, K. Chen *et al.*, "Near-field thermophotonic systems for low-grade waste-heat recovery," Nano Lett. **18**(8), 5224–5230 (2018).
[8]K. Chen, P. Santhanam, S. Sandhu *et al.*, "Heat-flux control and solid-state cooling by regulating chemical potential of photons in near-field electromagnetic heat transfer," Phys. Rev. B **91**(13), 134301 (2015).
[9]Y. De Wilde, F. Formanek, R. Carminati *et al.*, "Thermal radiation scanning tunnelling microscopy," Nature **444**(7120), 740–743 (2006).
[10]W. A. Challener, C. Peng, A. V. Itagi *et al.*, "Heat-assisted magnetic recording by a near-field transducer with efficient optical energy transfer," Nat. Photonics **3**(4), 220–224 (2009).
[11]J. C. Cuevas and F. J. García-Vidal, "Radiative heat transfer," ACS Photonics **5**(10), 3896–3915 (2018).
[12]P. Ben-Abdallah, S. A. Biehs, and K. Joulain, "Many-body radiative heat transfer theory," Phys. Rev. Lett. **107**(11), 114301 (2011).
[13]I. Latella, A. Pérez-Madrid, J. M. Rubi *et al.*, "Heat engine driven by photon tunneling in many-body systems," Phys. Rev. Appl. **4**(1), 011001 (2015).
[14]J. Dong, J. Zhao, and L. Liu, "Radiative heat transfer in many-body systems: Coupled electric and magnetic dipole approach," Phys. Rev. B **95**(12), 125411 (2017).
[15]L. Zhu, Y. Guo, and S. Fan, "Theory of many-body radiative heat transfer without the constraint of reciprocity," Phys. Rev. B **97**(9), 094302 (2018).
[16]P. Ben-Abdallah, "Thermal photon drag in many-body systems," Phys. Rev. B **99**(20), 201406 (2019).
[17]J. Song, L. Lu, B. Li *et al.*, "Thermal routing via near-field radiative heat transfer," Int. J. Heat Mass Transfer **150**, 119346 (2020).
[18]S. A. Biehs, R. Messina, P. S. Venkataram *et al.*, "Near-field radiative heat transfer in many-body systems," Rev. Mod. Phys. **93**(2), 025009 (2021).
[19]J. Song, Q. Cheng, B. Zhang *et al.*, "Many-body near-field radiative heat transfer: Methods, functionalities and applications," Rep. Prog. Phys. **84**(3), 036501 (2021).
[20]R. Messina, M. Antezza, and P. Ben-Abdallah, "Three-body amplification of photon heat tunneling," Phys. Rev. Lett. **109**(24), 244302 (2012).
[21]Y. H. Kan, C. Y. Zhao, and Z. M. Zhang, "Near-field radiative heat transfer in three-body systems with periodic structures," Phys. Rev. B **99**(3), 035433 (2019).
[22]J. Song, L. Lu, Q. Cheng *et al.*, "Three-body heat transfer between anisotropic magneto-dielectric hyperbolic metamaterials," J. Heat Transfer **140**(8), 082005 (2018).
[23]M. J. He, H. Qi, Y. Li *et al.*, "Graphene-mediated near field thermostat based on three-body photon tunneling," Int. J. Heat Mass Transfer **137**, 12–19 (2019).
[24]P. Ben-Abdallah and S. A. Biehs, "Near-field thermal transistor," Phys. Rev. Lett. **112**(4), 044301 (2014).
[25]Y. H. Kan, C. Y. Zhao, and Z. M. Zhang, "Enhancement and manipulation of near-field radiative heat transfer using an intermediate modulator," Phys. Rev. Appl. **13**(1), 014069 (2020).
[26]V. Kubytskyi, S. A. Biehs, and P. Ben-Abdallah, "Radiative bistability and thermal memory," Phys. Rev. Lett. **113**(7), 074301 (2014).
[27]X. Wu and C. Fu, "Near-field radiative modulator based on dissimilar hyperbolic materials with in-plane anisotropy," Int. J. Heat Mass Transfer **168**, 120908 (2021).
[28]P. Li, M. Lewin, A. V. Kretinin *et al.*, "Hyperbolic phonon-polaritons in boron nitride for near-field optical imaging and focusing," Nat. Commun. **6**(1), 7507 (2015).

[29]J. D. Caldwell, A. V. Kretinin, Y. Chen *et al.*, "Sub-diffractional volume-confined polaritons in the natural hyperbolic material hexagonal boron nitride," Nat. Commun. **5**(1), 5221 (2014).
[30]C. R. Dean, A. F. Young, I. Meric *et al.*, "Boron nitride substrates for high-quality graphene electronics," Nat. Nanotechnol. **5**(10), 722–726 (2010).
[31]L. Lu, B. Zhang, H. Ou *et al.*, "Enhanced near-field radiative heat transfer between graphene/hBN systems," Small **18**, 2108032 (2022).
[32]D. Feng, S. K. Yee, and Z. M. Zhang, "Near-field photonic thermal diode based on hBN and InSb films," Appl. Phys. Lett. **119**(18), 181111 (2021).
[33]K. Shi, F. Bao, and S. He, "Enhanced near-field thermal radiation based on multilayer graphene-hBN heterostructures," ACS Photonics **4**(4), 971–978 (2017).
[34]B. Zhao and Z. M. Zhang, "Perfect mid-infrared absorption by hybrid phonon-plasmon polaritons in hBN/metal-grating anisotropic structures," Int. J. Heat Mass Transfer **106**, 1025–1034 (2017).
[35]I. Latella, P. Ben-Abdallah, and M. Nikbakht, "Radiative thermal rectification in many-body systems," Phys. Rev. B **104**(4), 045410 (2021).
[36]L. Ferrari, C. Wu, D. Lepage *et al.*, "Hyperbolic metamaterials and their applications," Prog. Quantum Electron. **40**, 1–40 (2015).
[37]B. Lyu, H. Li, L. Jiang *et al.*, "Phonon polariton-assisted infrared nanoimaging of local strain in hexagonal boron nitride," Nano Lett. **19**(3), 1982–1989 (2019).
[38]G. T. Papadakis, C. J. Ciccarino, L. Fan *et al.*, "Deep-subwavelength thermal switch via resonant coupling in monolayer hexagonal boron nitride," Phys. Rev. Appl. **15**(5), 054002 (2021).
[39]R. Geick, C. H. Perry, and G. Rupprecht, "Normal modes in hexagonal boron nitride," Phys. Rev. **146**(2), 543 (1966).
[40]P. Yeh and M. Hendry, "Optical waves in layered media," Phys. Today **43**(1), 77 (1990).
[41]X. Liu, R. Z. Zhang, and Z. Zhang, "Near-perfect photon tunneling by hybridizing graphene plasmons and hyperbolic modes," ACS Photonics **1**(9), 785–789 (2014).
[42]K. Kloppstech, N. Könne, S.-A. Biehs *et al.*, "Giant heat transfer in the crossover regime between conduction and radiation," Nat. Commun. **8**(1), 14475 (2017).